Enhancing Biomarker Detection Sensitivity through Tag-Laser Induced Breakdown Spectroscopy with NELIBS

Ali Safi^{1*}, Joshua E. Landis¹, Helmar G. Adler¹, Hossein Khadem², Kemal Efe Esseller¹, Yuri Markushin³, Sara Honarparvaran⁴, Alessandro De Giacomo^{5,6}, Noureddine Melikechi^{1*}

Abstract:

Nanoparticle-enhanced laser-induced breakdown spectroscopy and Tag-LIBS are two approaches that have been shown to significantly enhance LIBS sensitivity and specificity. In an effort to combine both of these approaches, we have initiated a study on the effect of the presence of Silver nanoparticle concentrations on Europium (Eu) and Ytterbium (Yb) LIBS signals. We observe a signal enhancement of the emission lines of about 10 and 12 times for the Europium and Ytterbium lines. This study shows that Europium and Ytterbium are enhanced differently; Europium shows enhancement for both neutral and ionized species while the Ytterbium shows enhancement only for ionized species. Additionally, we found that NPs at 0.1 mg/mL and 0.05 mg/mL achieved maximum enhancement for Eu and Yb, respectively. Based on our findings, the temperature and electron density of Eu and Yb are not significantly different for NPs concentrations, but the total signal intensity is significantly higher for optimum NP concentrations for both Eu and Yb.

Keywords: Tag-LIBS, NELIBS, Antibody, Lanthanide Microparticle, Ag nanoparticle

¹ Department of Physics and Applied Physics, Kennedy College of Sciences, University of Massachusetts Lowell, MA 01854, USA

² Institute for Experimental Endocrinology and Oncology "Gaetano Salvatore" (IEOS), Second Unit, National Research Council, 80131, Napoli, Italy

³Optical Science Center for Applied Research, Delaware State University, 1200

N. Dupont Highway Dover, DE 19901, USA

⁴Student Research Committee, Fasa University of Medical Sciences, Fasa, Iran

⁵Department of Chemistry, University of Bari, Via Orabona 4, 70126 Bari, Italy

⁶Department of Chemistry, Kennedy College of Sciences, University of Massachusetts Lowell, MA 01854, USA

^{*}Corresponding author: Ali Safi@uml.edu

Introduction:

Laser-induced breakdown spectroscopy (LIBS) is an analytical technique that provides rapid, simultaneous quantitative and qualitative elemental analysis of any sample, regardless whether it is in a liquid, solid, or gas state[1]. The basic concepts of this method have been discussed and reviewed in numerous articles and books[2–5]. In brief, this technique is based on the analysis of the emission spectral lines of a laser-induced micro plasma generated by focusing a high-power laser pulse with appropriate wavelengths, energy, and pulse durations.

Recently, biomedical applications of LIBS have attracted attention. By using machine learning techniques for the analysis of LIBS spectra, researchers have reported promising differentiation accuracies between healthy controls and diseased ones[6,7]. Others have pursued approaches that provide elemental mapping, in vitro or ex vivo analysis of various biomedical samples including soft and hard tissues [8–11] Tag-LIBS is one such development. It is based on the tagging of metallic micro- or nanoparticles typically not present in biological samples to specific protein targets prior to conducting a LIBS analysis[12,13]. By capturing the LIBS spectrum of the tagged marker, the characteristic emission lines of the selected particles can be associated to the specific tagged protein. The first Tag-LIBS study was performed using silicon microparticles to detect cancer antigen, CA 125 [12] More recently, Tag-LIBS was used to detect simultaneously avidin tagged with Fe₂O₃ microparticles and CA125 tagged with Si microparticles¹³. This body of work shows that Tag-LIBS presents tremendous benefits in terms of sensitivity and specificity for simultaneously detecting multiple proteins using more than one set of micro-particles. Recently, Gondhalekar and co-workers reported the use of Tag-LIBS to develop paper-based assays for the detection of labeled biomolecules [14]. By labelling different analytes with lanthanides-complexed polymers, and then using LIBS, they were able to detect the presence of antibodies and bacteria in paper-based assays. Certain lanthanides have luminescence properties that make them attractive labels for bioassay methods and immunoassays [15-17]. Lanthanide ions possess long-lived luminescence, which make them attractive for time-resolved luminescence immunoassays for protein detection[18]. By utilizing yttrium-based upconversion nanoparticles (UCNP), Porizka et al developed Tag-LIBS as an alternative to Immunohistochemistry and Immunocytochemistry. Their results demonstrate that, using Tag-LIBS, breast cancer biomarkers (HER2) can be differentiated with high sensitivity and specificity [19].

While Tag-LIBS has recently emerged as a promising technique for biomedical applications, further improvements of its performance and possibly open new innovative approaches to develop it as a technique that can be used as a multiplexing assay. Previously, we used two metal microparticles as tags to detect the ovarian cancer biomarker leptin. ¹³ Multiple elemental marker micro-particle assays can potentially be used for the development of immunoassays and detection of numerous diseases (e.g., COVID-19, cancers, Alzheimer's) ¹³. This step will greatly benefit from enhancing Tag-LIBS signals for specific elements while preserving the simplicity of the approach. Similarly, while LIBS, in its different variants, has been used with success in many applications including space exploration[20], food analysis [21], pollution studies [21], increasing its sensitivity is highly desirable. In recent years, several researchers have implemented new experimental methods and reported improved LIBS sensitivity. These include double pulse

excitation [22,23], spatial confinement [24], magnetic confined LIBS[25], microwave enhancement LIBS [26], spark discharge LIBS[27]. Despite their successful application, the utilization of these techniques is limited due to the need for sophisticated instrumentation, and in some cases extensive sample manipulation.

One of the most promising developments to enhance the sensitivity of LIBS was recently proposed is nanoparticle-enhanced laser-induced breakdown spectroscopy (NELIBS) [28]. NELIBS involves the deposition of metallic nanoparticles (NPs), such as Ag and/or Au, on a sample surface before laser irradiation. De Giacomo and co-workers have shown that on metallic samples, this approach can yield 1-2 orders of magnitude enhancement. Further they applied NELIBS to biological samples including proteins, blood and amyloid fibrils detecting metals content in the range of ppb in a few µl of biological fluid [29–31].

We report here, for the first time, on a study aimed at improving the analytical capability of LIBS by bringing together Tag-LIBS and NELIBS using two lanthanide microparticles tagged to antibodies.

Sample preparation

Tagged sample:

To analyze samples consisting of metal-encoded antibodies, two standard labeled sets were used (Fluidigm). Antibody labeling with the lanthanide microparticles was performed using Maxpar® X8 Multimetal Labeling Kit (Fluidigm). After conjugation, the concentration of each antibody was adjusted to about 1 μ g/ μ l, and the conjugated antibodies were titrated for optimal concentration before experiments. The assay uses a water-soluble polymer with multiple metal-chelating ligands. The polymer has a maleimide group that can bind to cysteine -SH groups on the Fc part of an antibody. Attaching tags to antibodies through -SH groups (created by selectively reducing disulfide bonds) is known to better preserve antibody activity compared to randomly attaching tags to lysine's amino group. The chelating ligand is selected to form strong complexes with lanthanide (Ln³+) ions. The procedure of antibody labeling is summarized in Figure 1. A detailed description of the labeling procedure can be found in reference[32]. Essentially, X8 polymer was preloaded with the lanthanide of interest, and Tris(2-carboxyethyl) phosphine hydrochloride (TCEP) solution was used to partially reduce the purified carrier-free antibody under controlled time and temperature conditions. In the following steps, the antibody was conjugated to a lanthanide-loaded polymer. Following a few washes, it was ready for use.

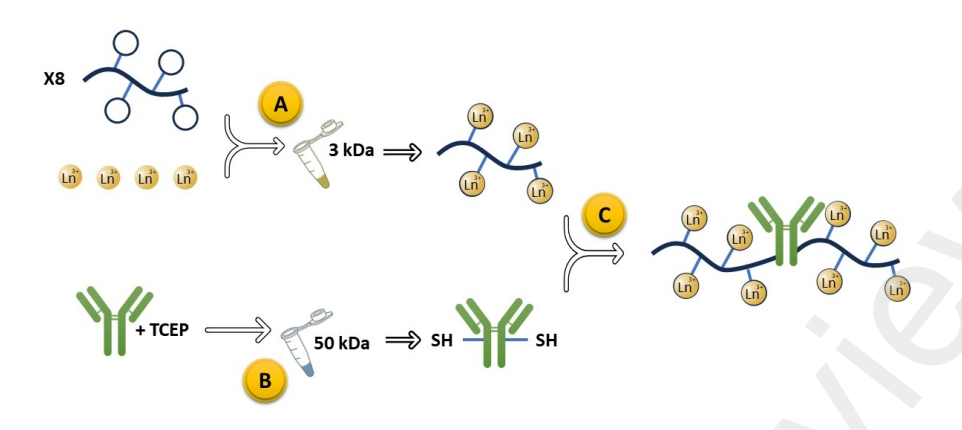


Figure 1: Schematic representation of the sequential steps involved in the labeling procedure. Step A: Loading the polymer with lanthanide. Step B: Partially reducing the antibody. Step C: Conjugating the antibody with the lanthanide-loaded polymer.

Ag solutions:

Figure 2 illustrates the properties of silver nanoparticles used in this study. The aqueous colloidal solution of citrate-stabilized silver nanoparticles (Nanocomposix) was characterized by transmission electron microscopy (TEM) shows a spherical morphology with a well-defined diameter of 20.1 ± 3.0 nm. The mass concentration of silver nanoparticles was measured using the inductively coupled plasma-mass spectrometry (ICP-MS) method, yielding a value of 1.08 mg/mL, which corresponds to a particle concentration of 2.4E+13 particles/mL. The absorbance spectrum of the silver nanoparticles exhibits a pronounced peak at 392 nm, attributed to the excitation of localized surface plasmon resonances (LSPRs). To explore the effect of NELIBS, a range of nanoparticle solutions was generated through stepwise dilution, resulting in concentrations spanning from 0.01 to 0.5 mg/mL.

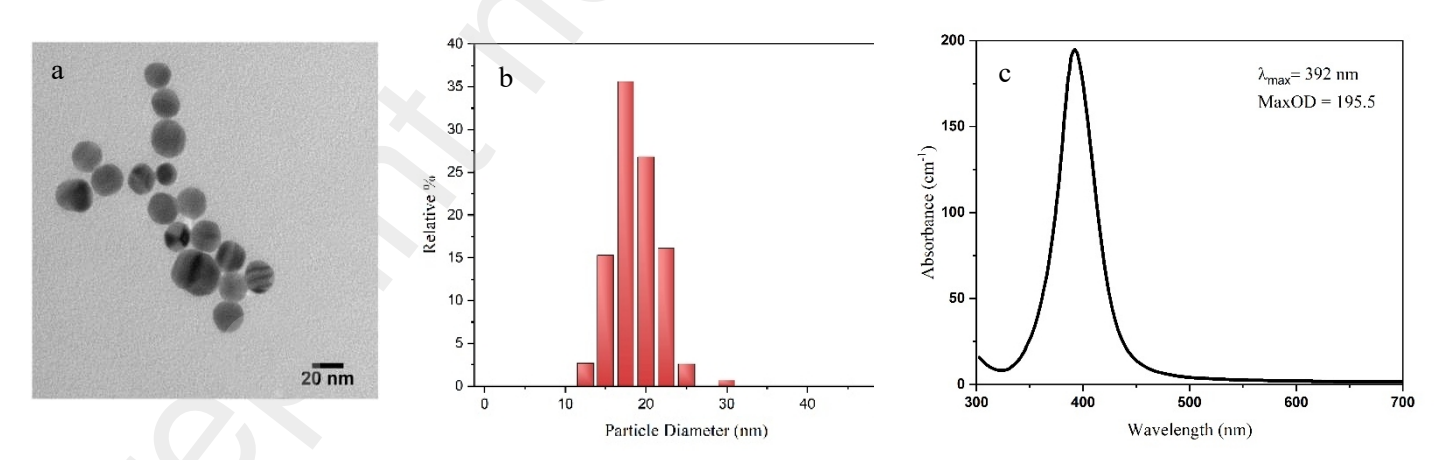


Figure 2: Silver nanoparticle characterization: a) the SEM image, b) Size distribution, c) UV-visible absorption spectrum of the Ag nanoparticles.

Experimental setup

The experimental setup used for this study is sketched in Figure 3. It consists of a Q-switched Nd-YAG laser (Continuum, Surelite II), operating at 1064 nm and pulse duration of 7 ns in air at atmospheric pressure. The laser beam was perpendicular to the target surface within a chamber (SciTrace, AtomTrace) and focused using an air-spaced doublet lens with a focal length of 30 mm. The chamber is equipped with a CMOS camera that provides a real-time view of the sample. As it was demonstrated that the NELIBS emission plasma volume is larger than that from LIBS, our optical detection system was adjusted to collect large area of plasma[33]. Plasma emission was collected through a lens with a focal distance of 44.5 mm coupled to 50 µm core-diameter optical fiber, at an angle of 45 degrees to the normal of the surface of the sample. To collect radiation from a larger area of the plasma, the distance between the lens and the plasma was set to be smaller than the focal length of the lens. The focused laser spot diameter was about 800 µm, the repetition rate of the laser was 0.5 Hz, and its energy was 130 ± 2 mJ. Emission spectra were acquired using Echelle spectrograph (Andor Technology, ME 5000) with a spectral range from 200 nm to 900 nm, coupled to a thermoelectrically cooled iStar Intensified Charge Coupled Device (ICCD) camera (Andor Technology, DH734-18F-03). A delay time of 1.5 us with respect to the laser pulse and a gate time of 5 µs was used for spectra detection. In this study, parafilm was tested to be used as an insulating substrate. We deposited 2 µl of Ag NPs solution on parafilm substrate which was previously rinsed in 2-propanol. Once the nanoparticle solution dried, 2 µl of the sample were deposited on it. Three different measurements were performed for each sample. As is typically the case in LIBS measurements, we eliminated the first shot (cleaning shot) and used the second and third to obtain an average spectrum which was used in our analysis.

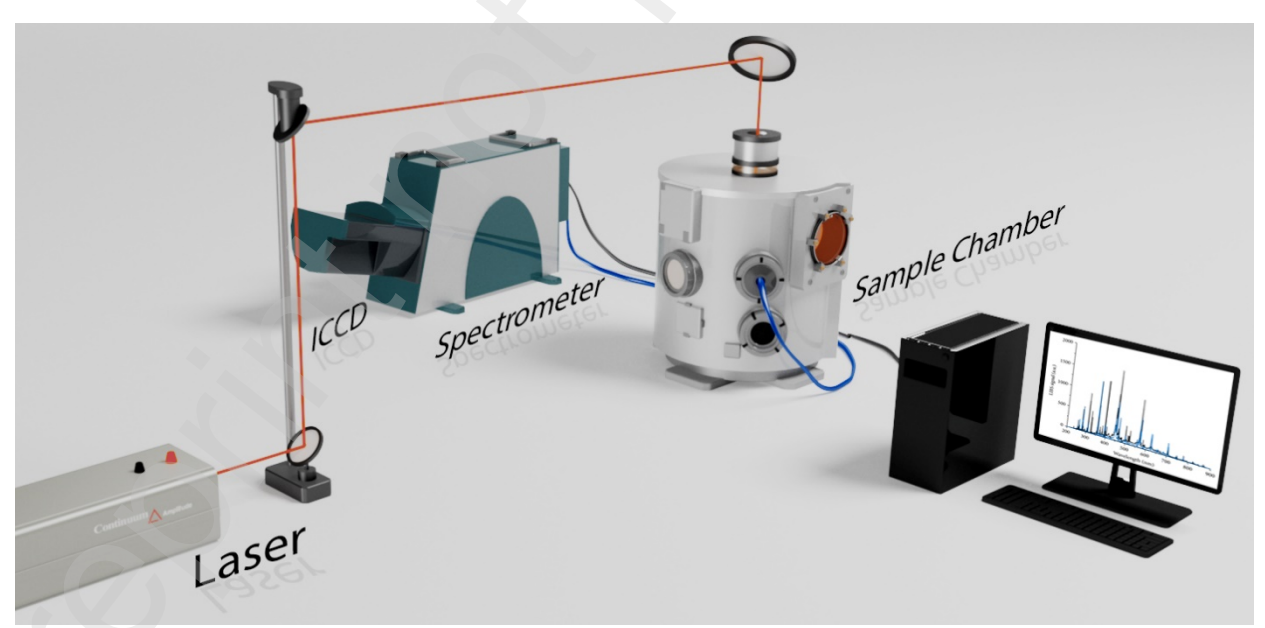


Figure 3: A schematic diagram illustrating the experimental setup, including the excitation source (Q-switched Nd-YAG Laser), sample chamber, optical components, and detection system (Echelle spectrometer and ICCD detector).

Results

a) Influence of nanoparticle deposition on LIBS intensity

We first investigated the effects of laser energy, nano particle size and concentration, timing parameters, collection optics, and substrate on the enhancement obtained [29]. We have found that parafilm as an insulator substrate, is more effective than metal substrates in reducing the spectral interference caused by the substrate. Furthermore, the use of non-hydrophobic substrates in NELIBS results in a coffee ring [34] which introduces spatial variations in the NPs distribution and leads to signal heterogeneity across the surface. To mitigate this issue, we used parafilm as a hydrophobic substrate[31]. The parafilm effectively minimizes the coffee ring effect, ensuring a more uniform distribution of analytes across the substrate surface.

To ensure that Ag NPs contribute to the laser induced plasma process, we have measured the intensities of various emission lines with various concentrations of nanoparticles. Figure 4.a shows the measured Ag signals at 546.5 nm for different concentrations of NPs. The NELIBS signal (LIBS signal was essentially buried in the noise) is obtained from integrating the area under the

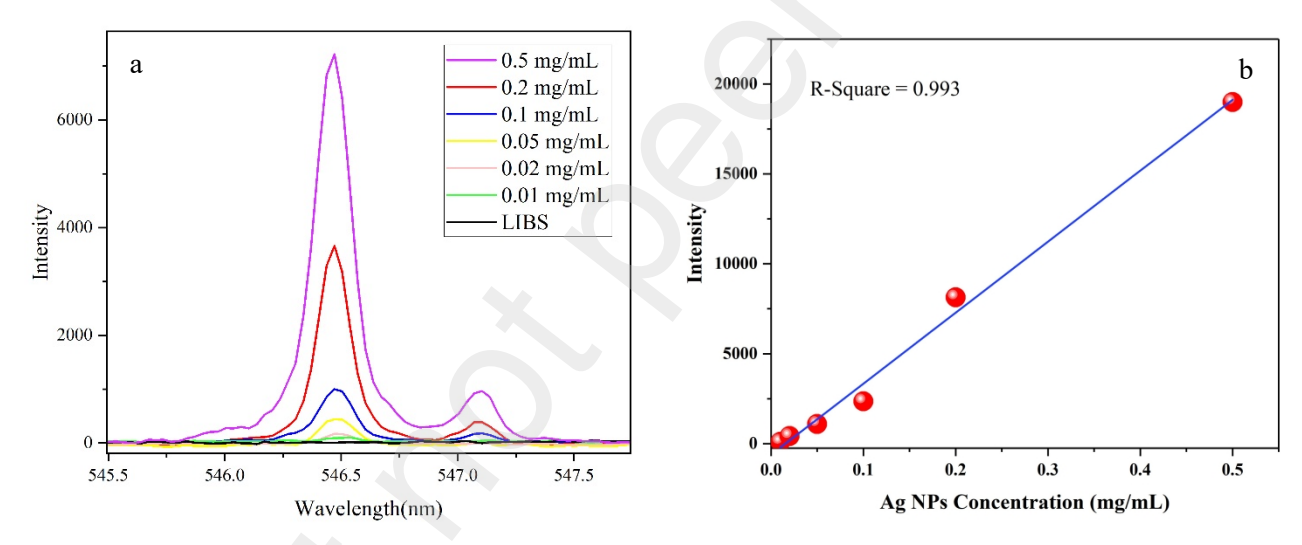


Figure 4: The intensity of the Ag line at 546.5 nm at different Ag NP concentrations. The uncertainty of the measurements is less than the diameter of each point in Figure 1.b.

line shape with background subtraction. The enhancement of the signal in NELIBS compared to LIBS is visible even at low concentration of silver NPs. A decrease in NPs concentration is associated with a decrease in Ag signal. Figure 4.b shows that the intensity of the emission line of Ag at 546 nm as a function of Ag NPs concentrations. This figure shows that there was no self-absorption for this spectral line[35]. The high coefficient of determination (R² = 0.993) further confirms the robustness of this correlation and implies that this emission line is a good candidate to calculate the electron density of the plasma. We note that some researchers used NPs surface concentrations rather than NPs solution concentrations which prompted us to calculate the concentration of nanoparticles on the sample's surface. This was performed using the sample view module in the Sci-Trace chamber (AtomTrace). We obtained 173±0.84, 66.5±7.7, 32.7±3.2, 16.8±1.4, 9.2±1.2, and 6.1±0.8 mg/cm² for NPs concentrations of 0.5, 0.2, 0.1, 0.05, 0.02, and 0.01

mg/mL, respectively and found that the surface concentration and the concentration of NPs had a linear correlation.

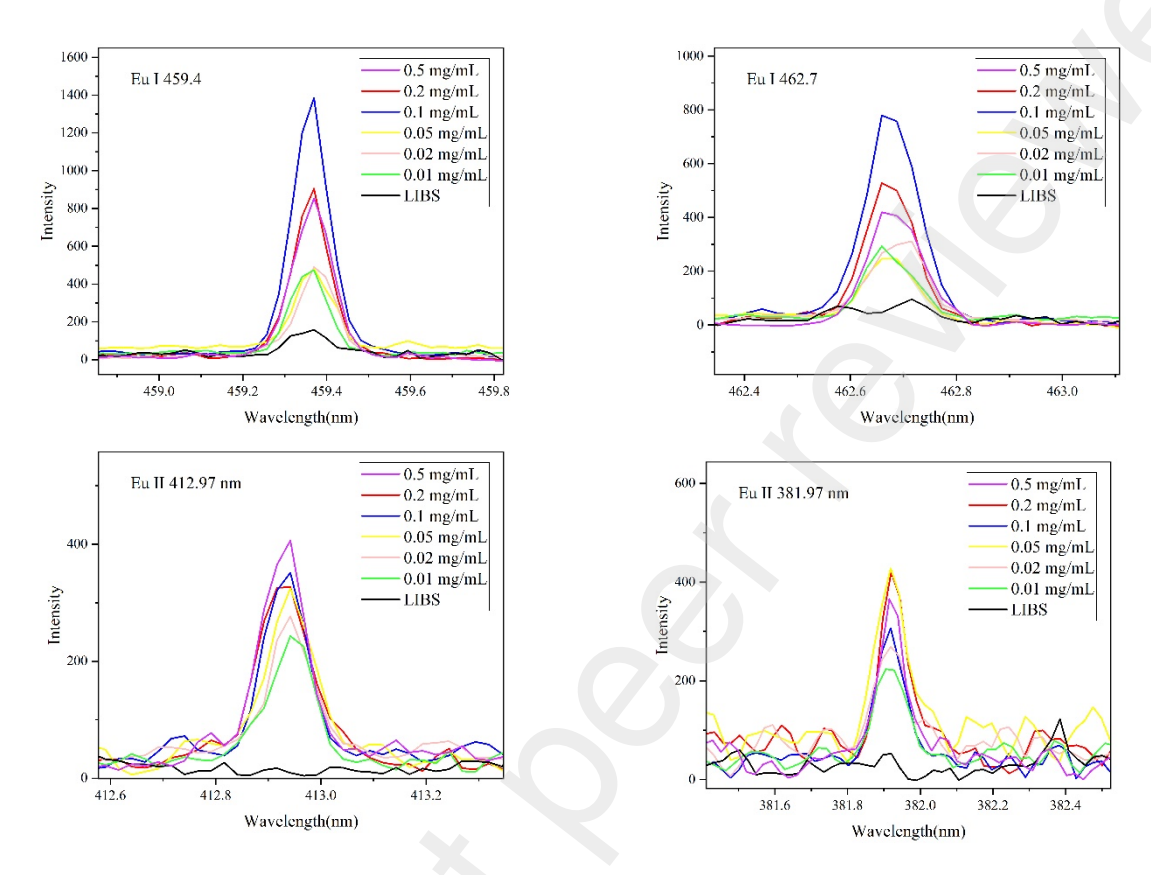


Figure 5:comparing Eu I and Eu II signals for LIBS and NELIBS in different Ag NPs concentrations. (The error bar was not significant enough to change the trend of the data.)

NELIBS signal enhancement depends on the concentration of NPs on the sample surface [36]. In an effort to determine the optimum concentration, we used 6 different Ag NPs solution concentrations. The results are shown in Figure 5 and Figure 6. Each sample was measured three times, with four shots per spot for each measurement. To avoid considering potentially contaminated spectra, only the average of the second and third shots were used in our analysis. We have observed that for all measurements, the NELIBS signal obtained with the second laser shot is stronger than the subsequent laser shots.

By comparing the emission line intensities obtained with NELIBS to that with LIBS, we observe that NELIBS yields higher signals at all different concentrations of Ag NPs tested. In addition,

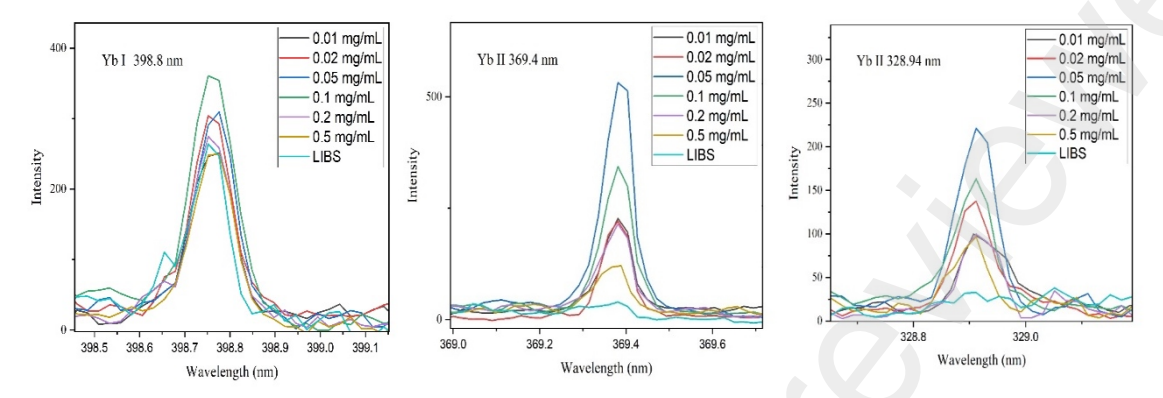


Figure 6: comparing Yb I and Yb II signals for LIBS and NELIBS in different Ag NPs concentrations. Show that the differences are statistically significant. (The error bar was not significant enough to change the trend of the data.)

Figure 5 shows that as the NP concentration is increased from 0.01 mg/mL to 0.5 mg/mL, for neutral Eu lines, the NELIBS signal grows to reach a maximum for a concentration of 0.1 mg/mL before dropping by about a factor of ten. In contrast, for Eu II lines no such a behavior was observed.

In Figure 6, we show the intensity of emission lines of Ytterbium (Yb) using NELIBS as a function of various concentrations of NPs. This Figure shows that neutral species behave differently from ionized species in NELIBS measurements. The Yb NELIBS signals obtained with various concentrations of Ag NPs resulted in a slight signal enhancement compared to LIBS measurements. NELIBS signal is almost the same for all Ag NPs concentrations. In contrast, ionized Yb displays a different behavior. We observe a significant enhancement with NELIBS measurements at all concentrations of Ag NPs compared to LIBS measurements. As can be seen from the figure, LIBS measurements have nearly no signal. However, both Yb emission lines at 328.94 nm and 369.4 nm display optimum enhancement for NELIBS measurements for a concentration of 0.05 mg/mL. There is also a significant improvement at a concentration of 0.1 mg/mL, similar to the Eu element.

b) Plasma temperature and density

To investigate the underlying mechanisms responsible for NELIBS, we have calculated the plasma temperature and electron density. A detailed explanation of the main mechanisms underlying NELIBS can be found in Ref [29].

The electron density of the plasma was determined by analyzing the line width of the neutral silver emission line at 546.55 nm using a formula represented by [18]:

$$\Delta \lambda_0 = \omega_s n_e$$

Here, $\Delta\lambda_0$ represents the full width at half maximum (FWHM) of the line and ω_s is the full-width Stark parameter of the line, which exhibits a weak dependence on both electron density and temperature [37]. This equation is based on Stark's broadening theory for non-hydrogenic atoms states, in which the width of a thin line is proportional to the plasma electron density [38]. As shown in Figure 4.b, the Ag line exhibits a linear relationship between the signal intensity and the concentration of Ag NPs, an indication that self-absorption does not occur for this spectral line and can therefore be used for electron density calculations. To measure line width, we fitted the emission line using pseudo-Voigt function, and deconvolved Gaussian instrumental broadening from the measured line width to obtain $\Delta\lambda_0$.

In Figure 7, we show the electron density as function of NPs concentration for Eu (left-hand vertical axis) and Yb (right-hand vertical axis). This Figure shows that, within the limit of our measurements (represented by the error bars shown in the figure), the electron density for both Eu and Yb are relatively unaffected by NPs concentrations and that their maximum values are obtained for concentrations of 0.1 and 0.05 mg/mL for Eu and Yb respectively. This result is consistent with those of the optimum NPs concentration measured when NELIBS enhancement was optimal. In fact, at 0.1 mg/mL, which corresponds to the maximum electron density for Eu, the highest enhancement (See Figure 5) is observed for the neutral lines of Eu. Similarly, for singly ionized lines of Yb at 0.05 maximum enhancement and electron density is observed (See Figure 6 and Figure 7). This suggests that optimum NELIBS enhancement may be accomplished by monitoring either neutral or ionized emission lines as a function of NP concentrations.

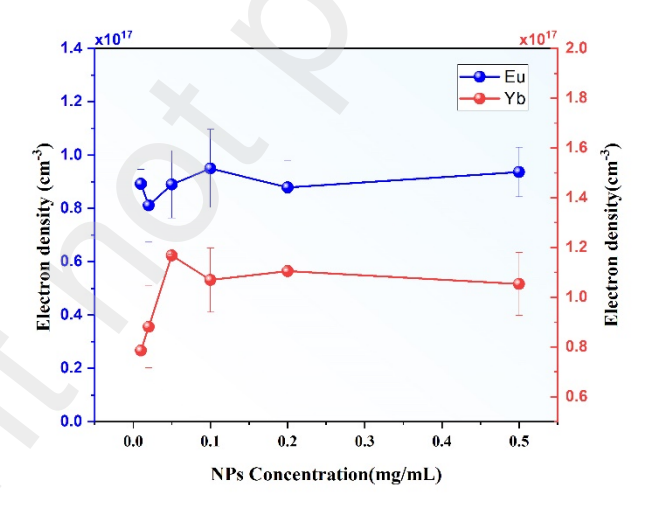


Figure 7:electron density vs NPs concentration for Eu and Yb

To calculate plasma temperature, we used the Saha-Boltzmann plot method [39]. The availability of spectral lines with slight differences in excitation energies of upper levels led us to use the Saha-Boltzmann method, in which lines from atoms and ions of the same element are included in the linear regression. Table 1 lists the atomic lines and their parameters used in calculating plasma temperature, for both Eu and Yb.

Table 1:spectral lines parameters used in calculating plasma temperature[40].

species	Wavelength (nm)	$E_i(cm^{-1})$	$E_k(cm^{-1})$	g_i	$oldsymbol{g}_k$	$A_{ki}(10^8\mathrm{s}^{-1})$
Yb I	398.8	0	25068.22	1	3	1.92
Yb II	369.42	0	27061.82	2	2	1.23
Yb II	328.94	0	30392.23	2	4	1.62
Eu I	4594.03	0	21761.26	8	10	1.61
Eu I	4627.22	0	21605.17	8	8	1.53
Eu I	4661.88	0	21444.58	8	6	1.45
Eu II	4205.05	0	23774.28	9	7	0.71
Eu II	4129.7	0	24207.86	9	9	0.68
Eu II	3819.67	0	26172.83	9	11	1.27
Eu II	3971.96	1669.21	26838.5	7	9	0.89

Figure 8 shows the Saha-Boltzmann plots of Yb element obtained in NELIBS measurements with different concentrations of Ag NPs and the calculated plasma temperatures of Eu and Yb. We note that, just as was the case for electron density, the plasma temperature remains relatively stable with NPs concentration for both elements. For both Eu and Yb, maximum plasma temperature was obtained when NELIBS measurements are performed with the NPs concentration of 0.05 mg/mL.

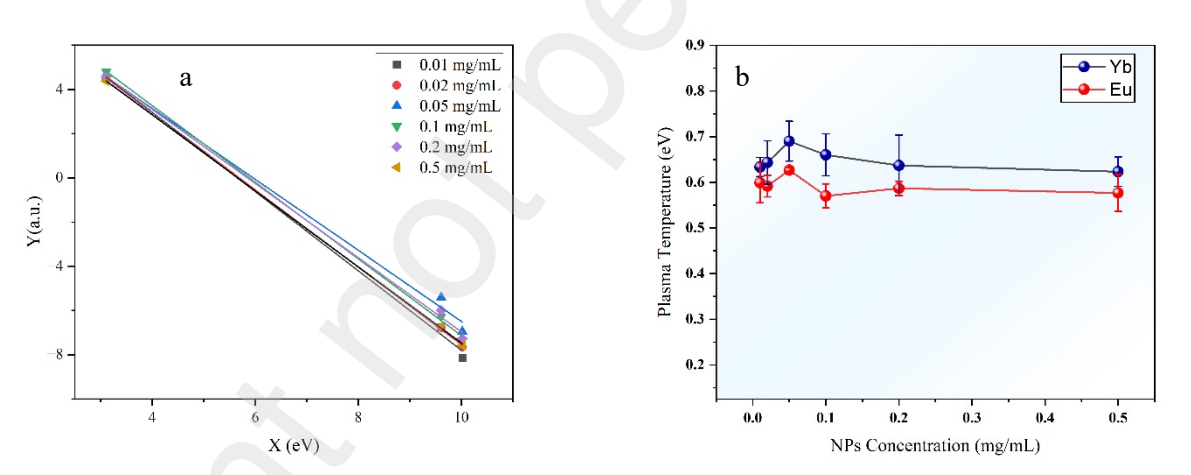


Figure 8: Saha-Boltzmann plot for Yb element by using three lines of Yb I 398.8, Yb II 369.42 and Yb II 328.94 b) Plasma temperature vs NPs concentration for Eu and Yb

We have observed that for Yb, the highest plasma temperature is reached for an NP concentration, of 0.05 mg/mL, that yields the maximum NELIBS enhancement for singly ionized Yb lines. For Eu, the results show that the lowest plasma temperature is obtained for an NP concentration of 0.1 mg/ml NP. This corresponds to the largest signal enhancement in NELIBS measurements for Eu neutral I emission lines as already observed in [41].

To investigate this observation further, we estimated the total intensity of the Eu and Yb spectral emission lines as a function of NPs concentration. This calculation was performed using the sum of neutral and first ionized of six Eu emission lines ($I^{Eu} = I_{I}^{Eu} + I_{II}^{Eu}$) and three Yb emission lines

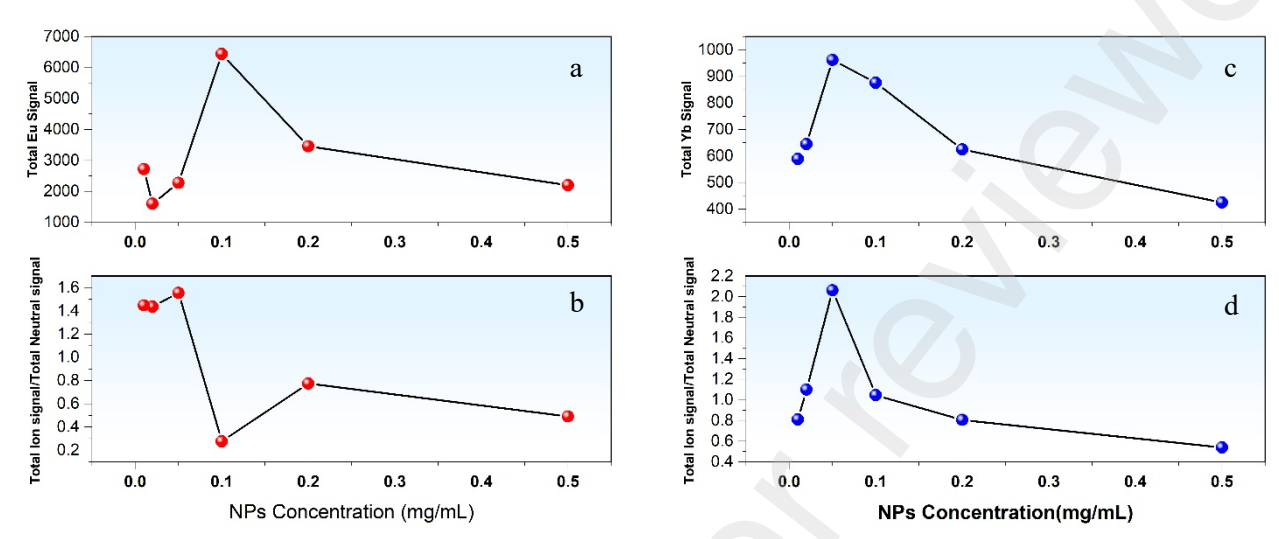


Figure 9: Total signal vs NPs concentration for a) Eu, c) Yb and Total Signal ratio of Ion to Neutral spectral lines for b) Eu, d)Yb

 $(I^{Yb} = I_I^{Yb} + I_{II}^{Yb})$. In addition, we calculated the ratio of the total signal of the ion lines to the total signal of the neutral spectral lines for Eu and for Yb. For Eu, three emission lines (459, 462, and 466 nm) were used to determine the total signal of neutral lines (I_I^{Eu}), and three lines (381, 412, and 420 nm) for the total signal of ion lines (I_{II}^{Eu}). For Yb, one emission line (398 nm) and two emission lines (328 and 369 nm) were used to calculate the intensity of neutral (I_I^{Yb}) and singly ionized Yb (I_{II}^{Yb}), respectively. For all calculations, emission line intensities were obtained by integrating the area under the line shape and subtracting the background. The results of these two calculations are shown in Figure 9.

Figure 9.a shows that, for Eu, the total signal intensity is significantly higher when the concentration is 0.1 mg/mL. This concentration is the one that also provided the optimum NELIBS enhancement as shown in Fig.3. However, Figure 9.b shows that, similar to plasma temperature value, minimum value of $\frac{I_{II}^{Eu}}{I_{I}^{Fu}}$ is obtained at 0.1 mg/mL, which implies that neutral species are more prevalent in the plasma formed from Eu. In the case of Yb, as shown in Figure 9.b and 8.d, the maximum value of total signal and ratio value of $\frac{I_{II}^{Yb}}{I_{I}^{Yb}}$ are obtained at 0.05 mg/mL, similar to what we observed for electron density and temperature during the analysis of Yb.

Discussion

This study reveals several points. First, our study has shown that employing lanthanide microparticles as tags for antibodies yields notable advantages. Indeed, the distinctive characteristics of lanthanides make them highly appealing markers for bioassay and immunoassay methods, enhancing specificity. Both ionized and neutral lines of Europium and Ytterbium were identified in LIBS signals, though the signal was not sufficiently strong. Additionally, in the case

of further investigation on blood samples, LIBS signals will not be affected by the lanthanoid elements due to their relatively low concentrations in the blood.

Second, Figure 5 and 6 show that for both Eu and Yb, the NELIBS emission lines of neutral and ionized species behave differently, reminiscent of an observation of LIBS emission lines of a C and Fe mixture [42]. We suspect that as Eu and Yb, have different atomic mass, ionization energy, heat of vaporization, and boiling temperature, which result in different plasma states, the temporal evolution and spatial distribution of the emitting species are different in the two cases. This leads to a signal enhancement that depends on time windows and plasma regions chosen for measurement. A spatially and temporally resolved plasma analysis is needed to better understand this observation.

Third, we have observed that for Eu, the minimum plasma temperature and $\frac{I_{II}^{Eu}}{I_{I}^{Eu}}$ are obtained at a concentration of 0.1 mg/mL. This corresponds to the highest signal enhancement. To analyze these observations, we note that under LTE condition, the ionization temperature, T_i , provides information about population densities of different ionization states and excited energy levels of both species [30]. It implies that:

$$T_i = T_{exc}^{ion} = T_{exc}^{neutral},$$

where T_{exc}^{ion} and $T_{exc}^{neutral}$ are excitation temperature of ionized and neutral species, respectively and can be calculated by Boltzmann plot method separately[44]. However, it was shown that this assumption can be satisfied only when measurements are performed using spatially resolved emission spectroscopy[45]. Use of integrated measurements in a not-fully homogeneous laser induced plasma may result in discrepancy between excitation and Boltzmann temperatures [46]. In fact, separated distributions of the neutral atom and ion densities, which result in different population-averaged values of temperature in spatially integrated measurements. Therefore, in this study, as measurements are performed in a spatially and temporally integrated approach, the calculated temperature can be considered as an apparent temperature that should not be identified with any of the local values of electron/excitation temperature in the plasma, but with the Boltzmann level population distribution along the optical path at the experimental conditions used for the measurement[46]. This apparent temperature primarily reflects the ratio of population densities between ionized and neutral species. Thus, for neutral Eu, plasma temperature and the ratio of $\frac{I_{T}^{E\mu}}{I_{T}^{E\mu}}$ has a minimum value. Besides, the cause behind the improvement observed in the Eu element at a concentration of 0.1 mg/mL cannot be attributed to plasma excitation temperature.

Fourth, it was previously reported that the use of a hydrophobic substrate, such as Parafilm, prevents the coffee ring effect and facilitates a more homogenous contribution of nanoparticles to the substrate. However, nanoparticles covering a hydrophobic substrate tend to cover a very small surface area in comparison non-hydrophobic substrate, after drying, resulting in a highly concentrated surface area. We found that the nanoparticle surface area varies between about 0.18 mm² and 0.32 mm², whereas the laser spot area on the surface was about 1.5 mm², indicating that almost 15-20 % of the surface has been exposed to NELIBS measurement. However, a significant

enhancement was obtained, and further enhancements expected using more NPs solutions. However, it should be noted using more NPs solutions may result in an inhomogeneous distribution of NPs on the surface.

We also assessed the repeatability of our measurements. While the error bars provide insight into the variability of our data, achieving greater repeatability than we have in this work is challenging. Variations can be introduced by factors such as size of nanoparticles, concentration and nanoparticles distribution on surfaces, and lasers and plasmas parameters. While the primary focus of this study was to increase sensitivity, we emphasize the importance of repeatability in NELIBS measurements.

Fifth, the absence of spectral lines in the LIBS measurement made it impossible to compare NELIBS and LIBS results in terms of plasma temperature and electron density. Instead, we have calculated plasma temperature and electron density for NELIBS measurements at different NPs concentrations. While the temperature and electron density for different concentrations are not significantly different, they depend on NPs concentrations. Despite maximum electron density at optimum concentrations (0.1mg/ml for Eu I and 0.05 for Yb II), plasma temperature calculated by the Saha-Boltzmann plot indicated different behavior. In fact, Eu is found to have a minimum temperature of 0.1 mg/mL, whereas Yb is found to have a maximum temperature at 0.05 mg/mL. We found that the maximum values for the total intensity of Eu and Yb spectral lines to be reached at optimum concentrations, similar to electron density. Consequently, additional mechanisms contribute to substantially increase the number of emitters at optimal NPs concentrations. This may be explained by more efficient atomization and excitation, as discussed in [41].

Conclusion

In summary, this work explored the potential of nanoparticle-enhanced laser-induced breakdown spectroscopy (NELIBS) in enhancing Tag-LIBS sensitivity. By optimizing silver nanoparticle concentration, significant signal enhancements were achieved for Europium (Eu) and Ytterbium (Yb) lines. Interestingly, distinct behaviors were observed for neutral and ionized species. For Eu, both neutral and ionized species exhibit considerable signal enhancement. However, for neutral species, strong NELIBS can be obtained at 0.1 mg/ml, while for ionized lines there is no clear trend. In the case of Yb, a significant NELIBS enhancement is observed for the ionized lines, whereas there is a slight improvement for the neutral lines. Combining NELIBS with Tag-LIBS can be utilized as an effective method of improving LIBS sensitivity and specificity in bioassays. Further studies in NETag-LIBS are needed to test the limits of this approach.

References

[1] L.J.R. Cremers, David A, Handbook of Laser-Induced Breakdown Spectroscopy, Wiley, 2006.

- [2] R. Noll, Laser-Induced Breakdown Spectroscopy, Springer Berlin Heidelberg, Berlin, Heidelberg, 2012. https://doi.org/10.1007/978-3-642-20668-9.
- [3] S.I. Miziolek AW, Palleschi V, Laser-Induced Breakdown Spectroscopy (LIBS), Cambridge University Press, Cambridge, 2006. https://doi.org/10.1017/CBO9780511541261.
- [4] D.W. Hahn, N. Omenetto, Laser-Induced Breakdown Spectroscopy (LIBS), Part II: Review of Instrumental and Methodological Approaches to Material Analysis and Applications to Different Fields, Appl. Spectrosc. 66 (2012) 347–419. https://doi.org/10.1366/11-06574.
- [5] D.W. Hahn, N. Omenetto, Laser-Induced Breakdown Spectroscopy (LIBS), Part I: Review of Basic Diagnostics and Plasma—Particle Interactions: Still-Challenging Issues within the Analytical Plasma Community, Appl. Spectrosc. 64 (2010) 335A-336A. https://doi.org/10.1366/000370210793561691.
- [6] N. Melikechi, Y. Markushin, D.C. Connolly, J. Lasue, E. Ewusi-Annan, S. Makrogiannis, Age-specific discrimination of blood plasma samples of healthy and ovarian cancer prone mice using laser-induced breakdown spectroscopy, Spectrochim. Acta Part B At. Spectrosc. 123 (2016) 33–41. https://doi.org/10.1016/j.sab.2016.07.008.
- [7] X. Chen, Y. Zhang, X. Li, Z. Yang, A. Liu, X. Yu, Diagnosis and staging of multiple myeloma using serum-based laser-induced breakdown spectroscopy combined with machine learning methods, Biomed. Opt. Express. 12 (2021) 3584. https://doi.org/10.1364/boe.421333.
- [8] D. Arabi, O. Hamdy, M.S.M. Mohamed, Z. Abdel-Salam, M. Abdel-Harith, Discriminating two bacteria via laser-induced breakdown spectroscopy and artificial neural network, AMB Express. 13 (2023). https://doi.org/10.1186/s13568-023-01569-0.
- [9] V. Gardette, V. Motto-Ros, C. Alvarez-Llamas, L. Sancey, L. Duponchel, B. Busser, Laser-Induced Breakdown Spectroscopy Imaging for Material and Biomedical Applications: Recent Advances and Future Perspectives, Anal. Chem. 95 (2023) 49–69. https://doi.org/10.1021/acs.analchem.2c04910.
- [10] R. Gaudiuso, N. Melikechi, Z.A. Abdel-Salam, M.A. Harith, V. Palleschi, V. Motto-Ros, B. Busser, Laser-induced breakdown spectroscopy for human and animal health: A review, Spectrochim. Acta Part B At. Spectrosc. 152 (2019) 123–148. https://doi.org/10.1016/j.sab.2018.11.006.
- [11] N. Melikechi, Optical Spectroscopy and Imaging for Cancer Diagnostics, WORLD SCIENTIFIC, 2023. https://doi.org/10.1142/12907.
- [12] Y. Markushin, N. Melikechi, Sensitive Detection of Epithelial Ovarian Cancer Biomarkers Using Tag-Laser Induced Breakdown Spectroscopy, in: S.A. Farghaly (Ed.), Ovarian Cancer, IntechOpen, Rijeka, 2012. https://doi.org/10.5772/28185.
- [13] N. Melikechi, Y. Markushin, Tag-laser-induced breakdown spectroscopy with Si, Ti, and Fe micro-particles and analysis of leptin in a phosphate buffer solution, Spectrochim. Acta Part B At. Spectrosc. 188 (2022) 106357. https://doi.org/10.1016/j.sab.2022.106357.
- [14] C. Gondhalekar, B. Rajwa, E. Bae, V. Patsekin, J. Sturgis, H. Kim, I.-J. Doh, P. Diwakar,

- J.P. Robinson, Multiplexed detection of lanthanides using laser-induced breakdown spectroscopy: a survey of data analysis techniques, in: Proc.SPIE, 2019: p. 1101609. https://doi.org/10.1117/12.2521453.
- [15] K. Matsumoto, Chapter 314 Recent developments in lanthanide chelates as luminescent labels for biomedical analyses, in: J.-C.G. Bünzli, V.K.B.T.-H. on the P. and C. of R.E. Pecharsky (Eds.), Incl. Actinides, Elsevier, 2020: pp. 119–191. https://doi.org/10.1016/bs.hpcre.2020.07.002.
- [16] X.-H. Chang, J. Zhang, L.-H. Wu, Y.-K. Peng, X.-Y. Yang, X.-L. Li, A.-J. Ma, J.-C. Ma, G.-Q. Chen, Research Progress of Near-Infrared Fluorescence Immunoassay, Micromachines. 10 (2019). https://doi.org/10.3390/mi10060422.
- [17] T. Steinkamp, U. Karst, Detection strategies for bioassays based on luminescent lanthanide complexes and signal amplification, Anal. Bioanal. Chem. 380 (2004) 24–30. https://doi.org/10.1007/s00216-004-2682-2.
- [18] A.K. Hagan, T. Zuchner, Lanthanide-based time-resolved luminescence immunoassays, Anal. Bioanal. Chem. 400 (2011) 2847–2864. https://doi.org/10.1007/s00216-011-5047-7.
- [19] P. Pořízka, K. Vytisková, R. Obořilová, M. Pastucha, I. Gábriš, J.C. Brandmeier, P. Modlitbová, H.H. Gorris, K. Novotný, P. Skládal, J. Kaiser, Z. Farka, Laser-induced breakdown spectroscopy as a readout method for immunocytochemistry with upconversion nanoparticles, Microchim. Acta. 188 (2021). https://doi.org/10.1007/s00604-021-04816-y.
- [20] S. Maurice, S.M. Clegg, R.C. Wiens, O. Gasnault, W. Rapin, O. Forni, A. Cousin, V. Sautter, N. Mangold, L. Le Deit, M. Nachon, R.B. Anderson, N.L. Lanza, C. Fabre, V. Payré, J. Lasue, P.-Y. Meslin, R.J. Léveillé, B.L. Barraclough, P. Beck, S.C. Bender, G. Berger, J.C. Bridges, N.T. Bridges, G. Dromart, M.D. Dyar, R. Francis, J. Frydenvang, B. Gondet, B.L. Ehlmann, K.E. Herkenhoff, J.R. Johnson, Y. Langevin, M.B. Madsen, N. Melikechi, J.-L. Lacour, S. Le Mouélic, E. Lewin, H.E. Newsom, A.M. Ollila, P. Pinet, S. Schröder, J.-B. Sirven, R.L. Tokar, M.J. Toplis, C. D'Uston, D.T. Vaniman, A.R. Vasavada, ChemCam activities and discoveries during the nominal mission of the Mars Science Laboratory in Gale crater, Mars, J. Anal. At. Spectrom. 31 (2016) 863–889. https://doi.org/10.1039/C5JA00417A.
- [21] M. Markiewicz-Keszycka, X. Cama-Moncunill, M.P. Casado-Gavalda, Y. Dixit, R. Cama-Moncunill, P.J. Cullen, C. Sullivan, Laser-induced breakdown spectroscopy (LIBS) for food analysis: A review, Trends Food Sci. Technol. 65 (2017) 80–93. https://doi.org/10.1016/j.tifs.2017.05.005.
- [22] Y. Nosrati, S.H. Tavassoli, M.M. Hassanimatin, A. Safi, Study of material ablation and plasma radiation in double-pulse laser induced breakdown spectroscopy at different delay times: Modeling and numerical simulation, Phys. Plasmas. 27 (2020). https://doi.org/10.1063/1.5132804.
- [23] A. Safi, M. Bahreini, S.H. Tavassoli, Comparative Study of Two Methods of Orthogonal Double-Pulse Laser-Induced Breakdown Spectroscopy of Aluminum, Opt. Spectrosc. 120 (2016) 367–378. https://doi.org/10.1134/S0030400X16030024.
- [24] X.K. Shen, J. Sun, H. Ling, Y.F. Lu, Spatial confinement effects in laser-induced

- breakdown spectroscopy, Appl. Phys. Lett. 91 (2007) 081501. https://doi.org/10.1063/1.2770772.
- [25] X.K. Shen, Y.F. Lu, T. Gebre, H. Ling, Y.X. Han, Optical emission in magnetically confined laser-induced breakdown spectroscopy, J. Appl. Phys. 100 (2006) 053303. https://doi.org/10.1063/1.2337169.
- [26] A. Khumaeni, T. Motonobu, A. Katsuaki, M. Masabumi, W. Ikuo, Enhancement of LIBS emission using antenna-coupled microwave, Opt. Express. 21 (2013) 29755–29768. https://doi.org/10.1364/OE.21.029755.
- [27] O.A. Nassef, H.E. Elsayed-Ali, Spark discharge assisted laser induced breakdown spectroscopy, Spectrochim. Acta Part B At. Spectrosc. 60 (2005) 1564–1572. https://doi.org/10.1016/j.sab.2005.10.010.
- [28] A. De Giacomo, R. Gaudiuso, C. Koral, M. Dell'Aglio, O. De Pascale, Nanoparticle-enhanced laser-induced breakdown spectroscopy of metallic samples, Anal. Chem. 85 (2013) 10180–10187. https://doi.org/10.1021/ac4016165.
- [29] M. Dell'Aglio, R. Alrifai, A. De Giacomo, Nanoparticle Enhanced Laser Induced Breakdown Spectroscopy (NELIBS), a first review, Spectrochim. Acta Part B At. Spectrosc. 148 (2018) 105–112. https://doi.org/10.1016/j.sab.2018.06.008.
- [30] A. De Giacomo, C. Koral, G. Valenza, R. Gaudiuso, M. Dell'Aglio, Nanoparticle Enhanced Laser-Induced Breakdown Spectroscopy for Microdrop Analysis at subppm Level, Anal. Chem. 88 (2016) 5251–5257. https://doi.org/10.1021/acs.analchem.6b00324.
- [31] M. Dell'Aglio, Z. Salajková, A. Mallardi, R. Mezzenga, L. van't Hag, N. Cioffi, G. Palazzo, A. De Giacomo, Application of gold nanoparticles embedded in the amyloids fibrils as enhancers in the laser induced breakdown spectroscopy for the metal quantification in microdroplets, Spectrochim. Acta Part B At. Spectrosc. 155 (2019) 115–122. https://doi.org/10.1016/j.sab.2019.04.002.
- [32] X. Lou, G. Zhang, I. Herrera, R. Kinach, O. Ornatsky, V. Baranov, M. Nitz, M.A. Winnik, Polymer-Based Elemental Tags for Sensitive Bioassays, Angew. Chemie Int. Ed. 46 (2007) 6111–6114. https://doi.org/10.1002/anie.200700796.
- [33] M. Dell'Aglio, C. Di Franco, A. De Giacomo, Different nanoparticle shapes for nanoparticle-enhanced laser-induced breakdown spectroscopy: nanosphere and nanorod effects, J. Anal. At. Spectrom. 38 (2023) 766–774. https://doi.org/10.1039/D2JA00324D.
- [34] M. Dell'Aglio, Z. Salajková, A. Mallardi, M.C. Sportelli, J. Kaiser, N. Cioffi, A. De Giacomo, Sensing nanoparticle-protein corona using nanoparticle enhanced Laser Induced Breakdown Spectroscopy signal enhancement, Talanta. 235 (2021) 122741. https://doi.org/10.1016/j.talanta.2021.122741.
- [35] F. Rezaei, G. Cristoforetti, E. Tognoni, S. Legnaioli, V. Palleschi, A. Safi, A review of the current analytical approaches for evaluating, compensating and exploiting self-absorption in Laser Induced Breakdown Spectroscopy, Spectrochim. Acta Part B At. Spectrosc. 169 (2020). https://doi.org/10.1016/j.sab.2020.105878.
- [36] F. Poggialini, B. Campanella, S. Giannarelli, E. Grifoni, S. Legnaioli, G. Lorenzetti, S.

- Pagnotta, A. Safi, V. Palleschi, Green-synthetized silver nanoparticles for Nanoparticle-Enhanced Laser Induced Breakdown Spectroscopy (NELIBS) using a mobile instrument, Spectrochim. Acta Part B At. Spectrosc. 141 (2018) 53–58. https://doi.org/10.1016/j.sab.2018.01.005.
- [37] A. Safi, S.M. Aberkane, A. Botto, B. Campanella, S. Legnaioli, F. Poggialini, S. Raneri, F. Rezaei, V. Palleschi, Determination of Spectroscopic Parameters of Ag(I) and Ag(II) Emission Lines Using Time-Independent Extended C-Sigma Method, Appl. Spectrosc. 75 (2021) 654–660. https://doi.org/10.1177/0003702821999425.
- [38] H.R. Griem, Spectral Line Broadening by Plasmas., Elsevier Science, 1974. https://books.google.com/books/about/Spectral_Line_Broadening_by_Plasmas.html?id=7 NO oUa37vUC (accessed June 17, 2023).
- [39] C. Aragón, J.A. Aguilera, Characterization of laser induced plasmas by optical emission spectroscopy: A review of experiments and methods, Spectrochim. Acta Part B At. Spectrosc. 63 (2008) 893–916. https://doi.org/10.1016/j.sab.2008.05.010.
- [40] NIST: Atomic Spectra Database Lines Form, (n.d.). https://physics.nist.gov/%0APhysRefData/ASD/lines form.html.
- [41] M. Dell'Aglio, A. Mallardi, R. Gaudiuso, A. De Giacomo, Plasma Parameters During Nanoparticle-Enhanced Laser-Induced Breakdown Spectroscopy (NELIBS) in the Presence of Nanoparticle-Protein Conjugates, Appl. Spectrosc. (2023). https://doi.org/10.1177/00037028231200511.
- [42] P. Sivakumar, L. Taleh, Y. Markushin, N. Melikechi, J. Lasue, An experimental observation of the different behavior of ionic and neutral lines of iron as a function of number density in a binary carbon–iron mixture, Spectrochim. Acta Part B At. Spectrosc. 82 (2013) 76–82. https://doi.org/10.1016/j.sab.2012.11.006.
- [43] G. Cristoforetti, A. De Giacomo, M. Dell'Aglio, S. Legnaioli, E. Tognoni, V. Palleschi, N. Omenetto, Local Thermodynamic Equilibrium in Laser-Induced Breakdown Spectroscopy: Beyond the McWhirter criterion, Spectrochim. Acta Part B At. Spectrosc. 65 (2010) 86–95. https://doi.org/10.1016/j.sab.2009.11.005.
- [44] G. Cristoforetti, E. Tognoni, L. a. Gizzi, Thermodynamic equilibrium states in laser-induced plasmas: From the general case to laser-induced breakdown spectroscopy plasmas, Spectrochim. Acta Part B At. Spectrosc. 90 (2013) 1–22. https://doi.org/10.1016/j.sab.2013.09.004.
- [45] J.. Aguilera, C. Aragón, Characterization of a laser-induced plasma by spatially resolved spectroscopy of neutral atom and ion emissions., Spectrochim. Acta Part B At. Spectrosc. 59 (2004) 1861–1876. https://doi.org/10.1016/j.sab.2004.08.003.
- [46] B. Bousquet, V. Gardette, V.M. Ros, R. Gaudiuso, M. Dell'Aglio, A. De Giacomo, Plasma excitation temperature obtained with Boltzmann plot method: Significance, precision, trueness and accuracy, Spectrochim. Acta Part B At. Spectrosc. 204 (2023) 106686. https://doi.org/10.1016/j.sab.2023.106686.